International Journal of Robotics and Control Systems
Vol. 5, No. 6, 2025, pp. 3435-3451
ISSN 2775-2658
http://pubs2.ascee.org/index.php/ijrcs

Design of A Terminal Sliding Mode Controller Based on Extended State Observer for Vehicle Control

Ali Aniss Ebrahim [a,1,*]

[a] Department of Industrial Automation, Faculty of Technical Engineering, University of Tartous, Syria
[1] ali.abuyaeel@gmail.com
* Corresponding Author

ARTICLE INFO

Article history
Received August 10, 2025
Revised October 04, 2025
Accepted January 15, 2026

Keywords
Nonlinear Vehicle Dynamics;
Extended State Observer;
Terminal Sliding Mode Control;
Robust Control;
Autonomous Vehicles

ABSTRACT

This paper aims to present a robust approach for controlling autonomous vehicles with nonlinear dynamics, addressing the key challenges of navigating in unknown environments and performing tasks under uncertain dynamics. Traditional approaches often exhibit limitations in handling uncertainty and convergence speed. To overcome these issues, this paper presents work on integrating a Terminal Sliding Mode Control (TSMC) with an Extended State Observer (ESO) to ensure finite-time convergence and active disturbance rejection. The proposed framework synergistically combines the TSMC controller and the ESO to achieve accurate trajectory tracking and robust disturbance rejection. The method is validated through MATLAB/Simulink simulations across multiple scenarios, confirming its effectiveness in navigating unknown environments under dynamic uncertainty. The proposed methodology demonstrates superior performance compared to traditional PID control. Key results indicate a nearly 60% reduction in settling time (to 1.3 seconds) and the complete elimination of overshoot in linear velocity tracking. Furthermore, the controller achieves approximately 78% higher tracking accuracy (RMSE 0.04 rad/s) while suppressing control vibrations by more than 75%. Meanwhile, ESO provides high-precision state estimation, converging in less than 0.6 seconds with an estimation error of less than 2.5%, and reconstructing system uncertainties with 70% higher accuracy than conventional methods. These results demonstrate that the proposed method is a superior and robust solution for high-performance autonomous vehicle applications operating under dynamic uncertainties and stringent real-time constraints.

1. Introduction

For several years, the trend has been increasing toward the widespread use of electric and autonomous vehicles. Intelligent transportation systems are undergoing a radical transformation, represented by the accelerated adoption of electric and autonomous vehicles, which have become essential components of the architecture of smart cities and future logistics systems [1]-[3]. This trend has extended to resource exploration and transportation in mining environments [4], [5]. The replacement of internal combustion engine vehicles with modern mobility solutions based on electricity and automation is a global trend aimed at enhancing sustainability and operational

efficiency [6]-[8]. However, realizing the full potential of these emerging technologies requires a deep understanding of their dynamics and the ability to enable robust, high-precision control to ensure safety and optimal performance under diverse operating conditions and with modeling uncertainty [9]-[11]. Accurately modeling the nonlinear and complex dynamics of autonomous vehicles represents a fundamental challenge in the design of control systems [12], [13]. In this regard, Terminal Slip Mode Control (TSMC) has emerged as a powerful framework for managing nonlinear systems, thanks to its intrinsic advantages such as finite-time convergence and superior disturbance rejection [14]-[16]. TSMC technology enables a control system to achieve near-zero tracking error within a limited time frame, even in the presence of uncertainty [17], [18]. In contrast, traditional linear control methodologies, such as transfer function analysis, remain insufficient to handle the nonlinear complexities inherent in smart vehicle systems [19], [20].

Despite their advantages, traditional TSMC controller implementations face significant challenges, most notably chatter, which leads to wear on mechanical components and performance degradation, especially when state variables approach the slip state [21]-[23]. To address these limitations, recent research has focused on developing hybrid control systems that combine the power of TSMC with advanced monitoring, estimation, and adaptation techniques. In this context, the use of an extended state observer (ESO) has proven remarkably effective in estimating and triggering real-time "total disturbances," which include unrepresented dynamics in models, parameter uncertainty, and external disturbances, allowing for compensation before they impact the system [24]-[26]. The combination of TSMC and ESO, in an architecture known as TSMC-based ESO, provides an advanced solution that combines the response speed of TSMC with the proactive compensation capability of ESO, resulting in effective vibration suppression and significant improvements in system robustness and tracking performance [27]-[29]. This hybrid approach has found successful applications in a wide range of autonomous platforms, including ground vehicles [30], [31] and multi-rotor UAVs [32], [33]. In addition, contemporary research is exploring other hybrid methodologies to enhance control robustness. For example, the incorporation of PID-based slip surfaces to improve dynamic performance under complex disturbances [34]. Simulations demonstrate superior performance over conventional SMCs in handling non-model dynamics and external disturbances. Furthermore, machine learning and reinforcement learning approaches are being combined to create adaptive controllers capable of self-tuning their parameters without the need for an accurate a priori model of the operating environment [35]-[37]. However, ensuring the stability of these indirect adaptive approaches remains a challenge, as documented in [38]. Reference [39] demonstrates that stability is not guaranteed when using an indirect adaptive fuzzy method to design a vehicle controller. While adaptive tuning of fuzzy rules can improve control loop performance against uncertainty and disturbances, stability is not guaranteed. Reference [40] also demonstrates that the robust H∞ design method reduces the impact of parameter uncertainty on control loop performance in the presence of disturbances. However, it cannot be used alone for effective vehicle control.

In practice, relying on expensive or impractical sensors to measure all state variables, such as lateral speed, represents a major obstacle [41], [42]. Therefore, the design of controllers based solely on output feedback (output feedback control) has received significant attention, aiming to achieve high performance with limited measurements (such as trajectory and direction), providing a better balance between cost and efficiency [43]-[45]. This paper leverages these recent developments to contribute to the presentation of a robust hybrid controller based on the Terminal Slide Module (TSMC) principle, integrating an Extended State Observer (ESO) into the output feedback architecture. The main goal is to achieve accurate and efficient trajectory tracking of a vehicle with nonlinear dynamics, while eliminating the need for expensive lateral speed sensors, reducing complexity and cost, and ensuring superior performance and effective vibration suppression.

2. Vehicle Dynamics

The vehicle dynamics is crucial to design a terminal sliding mode controller. The modeling follows Reference [46]. In vehicle dynamics, aerodynamic forces and external forces from tire-road

contact are significant. Therefore, analyzing these forces and torques is essential. Fig. 1 shows a schematic of the vehicle, which exhibits motion along the x, y, and z axes and rotation around these axes. The reference describes the dynamic equations for both deceleration and acceleration modes.

To ensure the proper performance of the presented method and obtain the desired results, a nonlinear model of the vehicle must be developed. With the exception of dynamic forces, all forces acting on the vehicle will be generated when the wheel comes into contact with the road. These factors must be taken seriously when modeling. In [47], a suitable nonlinear model of the vehicle was planned.

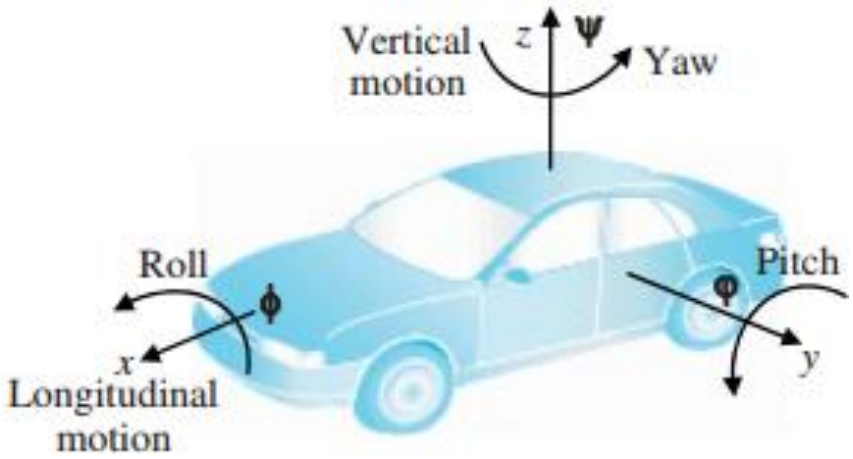

Fig. 1. Vehicle dynamics schematic

Longitudinal vehicle dynamics defines two distinct modes: acceleration ($Vw \geq Vv$), where traction forces from engine torque dominate, and deceleration ($Vw \leq Vv$), where braking forces and brake friction dominate. Each mode is modeled with a separate set of differential equations due to different powertrain physics [48]. This distinction is based on the wheel slip ratio and is fundamental to modern control systems such as anti-lock braking and traction control, especially in vehicles with single-wheel electric drive [49].

2.1. State Equations in Deceleration Mode ($Vw \leq Vv$)

Based on the reference [50], state-space equations (1) and (2) express the vehicle dynamics in deceleration mode.

$$\dot{V}_w = \alpha_1 M_m + \left[\alpha_2 + \alpha_3 \frac{V_w}{V_v} + \alpha_4 \, exp\left(\alpha \frac{V_w}{V_v}\right)\right]^{-1} \times \left[\alpha_5 + \alpha_6 \frac{V_w}{V_v} + \alpha_7 (V_v - V_a)^2 + \alpha_8 \frac{V_w}{V_v} (V_v - V_a)^2 + \alpha_9 exp\left(\alpha \frac{V_w}{V_v}\right) + \alpha_{10} (V_v - V_a)^2 \, exp\left(\alpha \frac{V_w}{V_v}\right)\right] \quad (1)$$

$$\dot{V}_v = \alpha_{11} + \alpha_{12} (V_v - V_a)^2 + \left[\alpha_2 + \alpha_3 \frac{V_w}{V_v} + \alpha_4 \, exp\left(\alpha \frac{V_w}{V_v}\right)\right]^{-1} \times \left[\alpha_{13} + \alpha_{14} \frac{V_w}{V_v} + \alpha_{14} (V_v - V_a)^2 + \alpha_{16} \frac{V_w}{V_v} (V_v - V_a)^2 + \alpha_{17} exp\left(\alpha \frac{V_w}{V_v}\right) + \alpha_{18} (V_v - V_a)^2 \, exp\left(\alpha \frac{V_w}{V_v}\right)\right] \quad (2)$$

The parameters in Equations (1) and (2) are listed in Table 1. By defining $u = M_m$, $x_1 = V_w$, and $x_2 = V_v$, the previous two equations can be rewritten as:

$$\begin{cases} \dot{x}_1 = \alpha_1 u + f_1(x_1, x_2) \\ \dot{x}_2 = f_2(x_1, x_2) \end{cases} \tag{3}$$

Table 1. Vehicle dynamic parameters in deceleration mode

Parameter	Nominal value	Parameter	Nominal value
α	C_2	α_{10}	$-\frac{1}{2}(1-\Psi)\rho SC_z k_v C_1 \exp(C_2)\, r_{eff}^2 /J$
α_1	$\frac{r_{eff}}{J}$	α_{11}	-gsinθ
α_2	$1+\chi k_v(C_1+C_3)$	α_{12}	$-\frac{1}{2M_v}\rho SC_x$
α_3	$-k_v\chi C_3$	α_{13}	$(1-\Psi)M_v g cos k_v(C_1+C_3)$
α_4	$-k_v\chi C_1 \exp(C_2)$	α_{14}	$-(1-\Psi)gcos\theta k_v C_3$
α_5	$-(1-\Psi)M_v gcos\theta\left(\mu_{rr}+k_v(C_1+C_3)\right) r_{eff}^2 /J$	α_{15}	$-\frac{1}{2M_v}(1-\Psi)\rho SC_Z k_v(C_1+C_3)$
α_6	$(1-\Psi)M_v gcos\theta k_v C_3 r_{eff}^2/J$	α_{16}	$\frac{1}{2M_v}(1-\Psi)\rho SC_Z k_v C_3$
α_7	$\frac{1}{2}(1-\Psi)\rho SC_z\left(\mu_{rr}+k_v(C_1+C_3)\right) r_{eff}^2/J$	α_{17}	$-(1-\Psi)gcos\theta\, C_1 \exp(C_2)$
α_8	$-\frac{1}{2}(1-\Psi)\rho SC_z k_v C_3 r_{eff}^2/J$	α_{18}	$\frac{1}{2M_v}(1-\Psi)\rho SC_Z k_v C_1 \exp(C_2)$
α_9	$(1-\Psi)M_v gcos\theta k_v C_1 \exp(C_2)\, r_{eff}^2/J$		

where Equations (3) is the state-space equations for the vehicle in deceleration mode. Knowing that $f_1(x_1, x_2)$ and $f_2(x_1, x_2)$ are defined as:

$$\begin{aligned} f_1(x_1,x_2) = & \left[\alpha_2 + \alpha_3\frac{x_1}{x_2} + \alpha_4\, exp\left(\alpha\frac{x_1}{x_2}\right)\right]^{-1} \times\left[\alpha_5 + \alpha_6\frac{x_1}{x_2}\right. \\ & + \alpha_7(x_2-V_a)^2 + \alpha_8\frac{x_1}{x_2}(x_2-V_a)^2 + \ \alpha_9 exp\left(\alpha\frac{x_1}{x_2}\right) \\ & \left. + \alpha_{10}\,(x_2-V_a)^2\, exp\left(\alpha\frac{x_1}{x_2}\right)\right] \end{aligned} \tag{4}$$

$$\begin{aligned} f_2(x_1,x_2) = & \ \alpha_{11} + \ \alpha_{12}(x_2-V_a)^2 \\ & + \left[\alpha_2 + \alpha_3\frac{x_1}{x_2} + \alpha_4\, exp\left(\alpha\frac{x_1}{x_2}\right)\right]^{-1} \times\left[\alpha_{13} + \alpha_{14}\frac{x_1}{x_2}\right. \\ & + \alpha_{14}(x_2-V_a)^2 + \alpha_{16}\frac{x_1}{x_2}(x_2-V_a)^2 + \ \alpha_{17} exp\left(\alpha\frac{x_1}{x_2}\right) \\ & \left. + \alpha_{18}\,(x_2-V_a)^2\, exp\left(\alpha\frac{x_1}{x_2}\right)\right] \end{aligned} \tag{5}$$

2.2. State Equations in Acceleration Mode ($Vw \geq Vv$)

Based on Reference [10], the state-space equations for acceleration mode can be written as (6) and (7).

$$\begin{aligned} \dot{V}_w = & \ \alpha'_1 M_m + \left[\alpha'_2 + \alpha'_3\frac{V_w}{V_v} + \alpha'_4\, exp\left(\alpha'\frac{V_w}{V_v}\right)\right]^{-1} \times\left[\alpha'_5 + \alpha'_6\frac{V_w}{V_v}\right. \\ & + \alpha'_7(V_v-V_a)^2 + \alpha'_8\frac{V_w}{V_v}(V_v-V_a)^2 + \ \alpha'_9 exp\left(\alpha\frac{V_w}{V_v}\right) \\ & \left. + \alpha'_{10}\,(V_v-V_a)^2\, exp\left(\alpha'\frac{V_w}{V_v}\right)\right] \end{aligned} \tag{6}$$

$$\begin{aligned}\dot{V}_v = {} & \alpha'_{11} + \alpha'_{12}(V_v - V_a)^2 \\ & + \left[\alpha'_2 + \alpha'_3 \frac{V_w}{V_v} + \alpha'_4 exp\left(\alpha' \frac{V_w}{V_v}\right)\right]^{-1} \times \left[\alpha'_{13} + \alpha'_{14} \frac{V_w}{V_v}\right. \\ & + \alpha'_{14}(V_v - V_a)^2 + \alpha'_{16} \frac{V_w}{V_v}(V_v - V_a)^2 + \alpha'_{17} exp\left(\alpha' \frac{V_w}{V_v}\right) \\ & \left. + \alpha'_{18}(V_v - V_a)^2 exp\left(\alpha' \frac{V_w}{V_v}\right)\right]\end{aligned} \tag{7}$$

The parameters in Equations (6) and (7) are listed in Table 2. By defining $u = M_m$, $x_1 = V_w$, and $x_2 = V_v$.

Table 2. Vehicle dynamic parameters during acceleration

Parameter	Nominal value	Parameter	Nominal value
α'	$-\boldsymbol{C_2}$	α'_{10}	$-\frac{1}{2}(1-\Psi)\rho \boldsymbol{SC_z k_v C_1} \exp(-\boldsymbol{C_2})\, \boldsymbol{r_{eff}^2/J}$
α'_1	$\frac{\boldsymbol{r_{eff}}}{\boldsymbol{J}}$	α'_{11}	$-\boldsymbol{g sin\theta}$
α'_2	$1 + \chi \boldsymbol{k_v}(\boldsymbol{C_1} + \boldsymbol{C_3})$	α'_{12}	$-\frac{1}{2\boldsymbol{M_v}}\rho \boldsymbol{SC_x}$
α'_3	$\boldsymbol{k_v \chi C_3}$	α'_{13}	$(1-\Psi)\boldsymbol{M_v g cos k_v}(\boldsymbol{C_1} - \boldsymbol{C_3})$
α'_4	$-\boldsymbol{k_v \chi C_1} \exp(\boldsymbol{C_2})$	α'_{14}	$(1-\Psi)\boldsymbol{g cos\theta k_v C_3}$
α'_5	$-(1-\Psi)\boldsymbol{M_v g cos\theta}\left(\mu_{rr} + \boldsymbol{k_v}(\boldsymbol{C_1} - \boldsymbol{C_3})\right) \boldsymbol{r_{eff}^2/J}$	α'_{15}	$-\frac{1}{2\boldsymbol{M_v}}(1-\Psi)\rho \boldsymbol{SC_Z k_v}(\boldsymbol{C_1} - \boldsymbol{C_3})$
α'_6	$-(1-\Psi)\boldsymbol{M_v g cos\theta k_v C_3 r_{eff}^2/J}$	α'_{16}	$-\frac{1}{2\boldsymbol{M_v}}(1-\Psi)\rho \boldsymbol{SC_Z k_v C_3}$
α'_7	$\frac{1}{2}(1-\Psi)\rho \boldsymbol{SC_z}\left(\mu_{rr} + \boldsymbol{k_v}(\boldsymbol{C_1} - \boldsymbol{C_3})\right) \boldsymbol{r_{eff}^2/J}$	α'_{17}	$-(1-\Psi)\boldsymbol{g cos\theta}\, \boldsymbol{C_1} \exp(-\boldsymbol{C_2})$
α'_8	$\frac{1}{2}(1-\Psi)\rho \boldsymbol{SC_z k_v C_3 r_{eff}^2/J}$	α'_{18}	$\frac{1}{2\boldsymbol{M_v}}(1-\Psi)\rho \boldsymbol{SC_Z k_v C_1} \exp(-\boldsymbol{C_2})$
α'_9	$(1-\Psi)\boldsymbol{M_v g cos\theta k_v C_1} \exp(-\boldsymbol{C_2})\, \boldsymbol{r_{eff}^2/J}$		

The previous two equations can be rewritten as follows:

$$\begin{cases}\dot{x}_1 = \alpha'_1 u + f'_1(x_1, x_2) \\ \dot{x}_1 = f'_2(x_1, x_2)\end{cases} \tag{8}$$

where $f'_1(x_1, x_2)$ and $f'_2(x_1, x_2)$ are defined as:

$$\begin{aligned}f'_1(x_1, x_2) = {} & \left[\alpha'_2 + \alpha'_3 \frac{x_1}{x_2} + \alpha'_4 exp\left(\alpha' \frac{x_1}{x_2}\right)\right]^{-1} \times \left[\alpha'_5 + \alpha'_6 \frac{x_1}{x_2}\right. \\ & + \alpha'_7(x_2 - V_a)^2 + \alpha'_8 \frac{x_1}{x_2}(x_2 - V_a)^2 + \alpha'_9 exp\left(\alpha' \frac{x_1}{x_2}\right) \\ & \left. + \alpha'_{10}(x_2 - V_a)^2 exp\left(\alpha' \frac{x_1}{x_2}\right)\right]\end{aligned} \tag{9}$$

$$\begin{aligned}f'_2(x_1, x_2) = {} & \alpha'_{11} + \alpha'_{12}(x_2 - V_a)^2 \\ & + \left[\alpha'_2 + \alpha'_3 \frac{x_1}{x_2} + \alpha'_4 exp\left(\alpha' \frac{x_1}{x_2}\right)\right]^{-1} \times \left[\alpha'_{13} + \alpha'_{14} \frac{x_1}{x_2}\right. \\ & + \alpha'_{14}(x_2 - V_a)^2 + \alpha'_{16} \frac{x_1}{x_2}(x_2 - V_a)^2 + \alpha'_{17} exp\left(\alpha' \frac{x_1}{x_2}\right) \\ & \left. + \alpha'_{18}(x_2 - V_a)^2 exp\left(\alpha' \frac{x_1}{x_2}\right)\right]\end{aligned} \tag{10}$$

2.3. Comprehensive State Equations of Vehicle Dynamics

This section integrates the state-space equations for both deceleration and acceleration modes to design the terminal sliding mode controller. The comprehensive state equations are given by (11), where other parameters are defined in (12) to (15).

$$\begin{cases} \dot{x}_1 = \alpha_1^*(x_1, x_2)u + g_1(x_1, x_2) \\ \dot{x}_2 = g_2(x_1, x_2) \end{cases} \tag{11}$$

$$g_1(x_1, x_2) = \sigma(x_1, x_2) f_1(x_1, x_2) + \big(1 - \sigma(x_1, x_2)\big) f'_1(x_1, x_2) \tag{12}$$

$$g_2(x_1, x_2) = \sigma(x_1, x_2) f_2(x_1, x_2) + \big(1 - \sigma(x_1, x_2)\big) f'_2(x_1, x_2) \tag{13}$$

$$\alpha_1^*(x_1, x_2) = \sigma(x_1, x_2)\alpha_1 + \big(1 - \sigma(x_1, x_2)\big)\alpha'_1 \tag{14}$$

$$\sigma(x_1, x_2) = \begin{cases} 1 & x_1 \le x_2 \\ 0 & x_1 > x_2 \end{cases} \tag{15}$$

3. Proposed Controller Methodology

Fig. 2 shows the schematic of the proposed controller. This schematic represents an advanced vehicle control system based on the combination of a terminal slip controller (TSMC) and an extended state monitor (ESO). The ESO plays a vital role in estimating the unmeasured internal state of the vehicle, as well as estimating the "total disturbance," which includes model uncertainty and external disturbances. The TSMC controller then utilizes these estimates to generate a robust control signal that not only corrects the error but also proactively cancels the effect of the estimated disturbance.

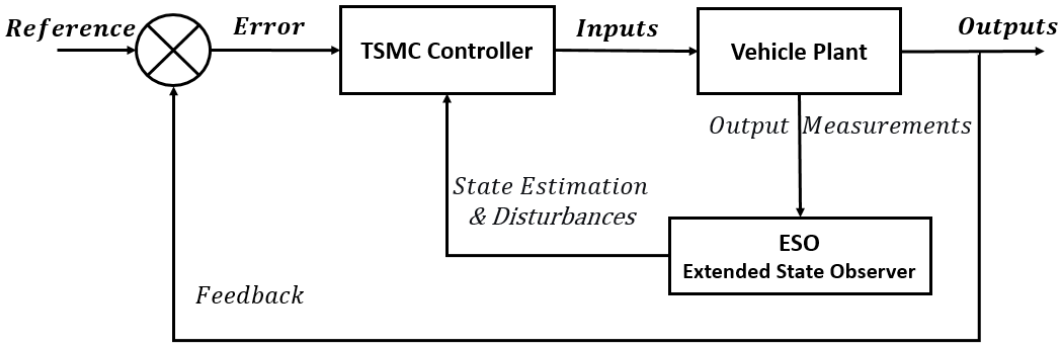

Fig. 2. Block diagram of the presented methodology

The controller will be explained through the mathematical relationships of both the Terminal sliding Mode Controller (TSMC) and Extended State Observer (ESO) incorporated in our approach to ensure finite-time convergence and disturbance rejection.

4. Terminal Sliding Mode Controller

A main characteristic of sliding mode control is its robustness against uncertainty and disturbances in nonlinear systems. A nonlinear system is represented by (16), where $x \in R^n$ is the state vector, $u \in R^m$ is the input vector, $f(x) \in R^n$ and $g(x) \in R^{n \times m}$ are nonlinear functions, $\Delta f(x)$ and $\Delta g(x)$ describe system uncertainties, and $d(t)$ represents disturbances.

To enhance convergence and finite-time stability, Terminal Sliding Mode Control (TSMC) introduces a nonlinear sliding surface that forces system states to reach equilibrium in finite time, unlike conventional SMC which achieves asymptotic convergence. This approach significantly improves robustness against the matched uncertainties ($\Delta f(x)$, $\Delta g(x)$) and disturbances ($d(t)$) specified in (16), while reducing chattering through continuous approximation techniques [51].

$$\dot{x} = f(x) + \Delta f(x) + \big(g(x) + \Delta g(x)\big)u + d(t) \tag{16}$$

The disturbance dynamics are assumed to satisfy the Lipschitz condition with coefficient L_i, where the Lipschitz condition is a mathematical assumption that limits the rate of change of the function, ensuring that the perturbations and uncertainties in the system cannot change at an infinite speed, which is crucial for the stability analysis and design of robust controllers [52], [53], as shown in (17).

$$\Psi = \Delta f + \Delta g + d \tag{17}$$

To design the terminal sliding mode controller, the sliding surface is defined as (18), where $e = x - x_d$, $k_1 = diag(k_{11}, \dots, k_{1n})$, $k_2 = diag(k_{21}, \dots, k_{2n})$, $k_{ij} > 0$, $\gamma_1 \geq 1$, and $0 < \gamma_2 < 1$.

$$s = e + \int_0^t \left(k_1 sig^{\gamma_1}(e) + k_2 sig^{\gamma_2}(e)\right) d\tau \tag{18}$$

When the error reaches the sliding surface, the dynamics $\dot{s} = 0$ hold. Thus, the error dynamics on the sliding surface are given by (19).

$$\dot{e} = -k_1 sig^{\gamma_1}(e) - k_2 sig^{\gamma_2}(e) \tag{19}$$

Solving the differential equations in (19) shows that the error $e = x - x_d$ converges to zero in finite time. The structure of the terminal sliding mode controller is given by (20), where $l_1 = diag(l_{11}, \dots, l_{1n})$, $l_2 = diag(l_{21}, \dots, l_{2n})$, and $0 < \eta < 1$.

$$u = -g^{-1}[f - \dot{x}_d + k_1 sig^{\gamma_1}(e) + k_2 sig^{\gamma_2}(e) - l_1 s + l_2 sig^{\eta}(s)] \tag{20}$$

4.1. Stability Proof

This section proves the stability of the proposed terminal sliding mode controller using the Lyapunov function (21), where s is the sliding surface.

$$V = \frac{1}{2} s s^T \tag{21}$$

Proving stability using the Lyapunov function is a powerful methodology to ensure the robustness of the controller in the presence of uncertainties and perturbations, where the design of the sliding surface ensures that the trajectories converge to the sliding region in finite time [48].

The derivative of the Lyapunov function on the sliding surface is given by (22), and the sliding surface derivative is defined in (23).

$$\dot{V} = s^T \dot{s} \tag{22}$$

$$\dot{s} = l_1 s - l_2 sig^n(s) \tag{23}$$

Using (23), (22) can be rewritten as (24), where $\bar{l}_1 = \max\{l_{1i}\}$ and $\underline{l}_2 = \min\{l_{2i}\}$.

$$\dot{V} = s^T[l_1 s - l_2 sig^n(s)] = s^T l_1 s - s^T l_2 sig^n(s) \leq \bar{l}_1 \|s\|^{\eta+1} - \underline{l}_2 \|s\|^{\eta+1} = 2\bar{l}_1 V - 2^{\frac{\eta+1}{2}} \underline{l}_2 V^{\frac{\eta+1}{2}} \tag{24}$$

From (24), the time T for the state variables to reach the sliding surface is given by (25), proving the controller's stability.

$$T \leq \frac{ln\left(\frac{\underline{l}_2 - 2^{\left(\frac{1-\eta}{2}\right)} \bar{l}_1 V^{\left(\frac{1-\eta}{2}\right)}}{\underline{l}_2}\right)}{\bar{l}_1 (1-\eta)} \tag{25}$$

To estimate uncertainty and disturbances, an extended state observer is introduced. Let $z = [z_1, z_2, \dots, z_m]$ be the estimate of the disturbance and uncertainty vector $\hat{\Psi}$. The control input is then modified as (26).

$$u = -g^{-1}[f - \dot{x}_d + k_1 sig^{\gamma_1}(e) + k_2 sig^{\gamma_2}(e) - l_1 s + l_2 sig^{\eta}(s) + z] \tag{26}$$

5. Extended State Observer

The generalized state observer (ESO) estimates the state vector of nonlinear systems. Consider a nonlinear system with dynamics (27), where x_1 to x_n are state variables, $f(.)$ is a nonlinear function, $u(t)$ is the control input, $y(t)$ is the measurement vector, and $\omega(t)$ is an unknown disturbance.

$$\begin{gathered} \dot{x}_1 = x_2 \\ \vdots \\ \dot{x}_n = f(t, x_1, x_2, \dots, x_n) + \omega(t) + bu(t) \\ y = x_1 \end{gathered} \tag{27}$$

The ESO operating principle is based on considering both the nonlinear function $f(.)$ and the disturbance $\omega(t)$ as a total disturbance, and the system state is expanded to include this disturbance as a new state $x\{n+1\} = f(.) + \omega(t)$. A nonlinear observer (such as a modified Lüneberger observer) is then designed to estimate all system states $x_1, x_2, \dots, x_n$ as well as the total disturbance state $x\_\{n+1\}$ in real time [54]. Recent research [55] has shown that this approach is effective even when the nonlinear dynamics f(.) is not fully known, making it robust against model uncertainty and external disturbances.

5.1. Observer Design with Known System Dynamics

The basic principle of this method is to assume that the perturbation ω(t) has its own dynamics. The simplest model is to assume that its time derivative $h(t)$ is unknown but finite, i.e., $\dot{\omega}(t) = h(t)$ [56]. This practically reasonable assumption allows the equations of state to be rewritten as (28), where the perturbation $x_{n+1} = \omega(t)$ becomes an additional state, and $h(t)$ represents the uncertainty and perturbations.

$$\begin{gathered} \dot{x}_1 = x_2 \\ \vdots \\ \dot{x}_n = f(t, x_1, x_2, \dots, x_n) + x_{n+1} + bu(t) \\ \dot{x}_{n+1} = h(t) \\ y = x_1 \end{gathered} \tag{28}$$

The generalized state observer is designed as (29), where z_i and β_i are state estimates and observer gains, respectively. It is important to note that the real secret behind the performance of this observer depends on the choice of the nonlinear correction functions $g_i(\varepsilon)$ [57].

$$\begin{gathered} \varepsilon(t) = z_1(t) - y(t) \\ \dot{z}_1(t) = z_2(t) - \beta_1 g_1(\varepsilon(t)) \\ \vdots \\ \dot{z}_n(t) = z_{n+1}(t) + f(t, z_1, z_2, \dots, z_n) - \beta_n g_n\big(\varepsilon(t)\big) + bu(t) \end{gathered} \tag{29}$$

$$\dot{z}_{n+1} = -\beta_{n+1} g_{n+1}(z_1 - y(t))$$

The function $g_i(.)$ is defined in (30), where $a \in (0,1)$, $a = (m/2n)$ $(n = 1,2, \dots \; and \; m < 2n)$ (typically 0.5) and δ is set to 1% of the output range.

$$g_i(\varepsilon, a, \delta) = \begin{cases} |\varepsilon|^a sign(\varepsilon) & \varepsilon < \delta \\ \dfrac{\varepsilon}{\delta^{1-a}} & |\varepsilon| \geq \delta \end{cases} \tag{30}$$

5.2. Observer Design for Nonlinear Vehicle Dynamics

The vehicle dynamics with uncertainty are given by:

$$\begin{cases} \dot{x}_1 = \alpha_1^*(x_1, x_2)u + g_1(x_1, x_2) + \Delta g_1 \\ \dot{x}_2 = g_2(x_1, x_2) + \Delta g_2 \end{cases} \tag{31}$$

To overcome the challenges of uncertainties Δg_1 andΔg_2, a state augmentation strategy is used [58], [59]. The basic idea is to treat these uncertainties as additional unmeasured states that the observer must estimate. This transforms the disturbance estimation problem into a standard state estimation problem for an extended system.

where Δg_1 and Δg_2 represent uncertainties in x_1 and x_2, respectively. Define $\bar{z}_1$ and $\bar{z}_2$ as (32), where z_1 estimates x_1, z_2 estimates x_2, z_3 estimates Δg_1, and z_4 estimates Δg_2.

$$\bar{z}_1 = \begin{bmatrix} z_1 \\ z_2 \end{bmatrix}, \qquad \bar{z}_2 = \begin{bmatrix} z_3 \\ z_4 \end{bmatrix} \tag{32}$$

The observer is then designed as (33), where $y(t)$ is defined in (34).

$$\begin{aligned} \varepsilon(t) &= z_1(t) - y(t) \\ \dot{\bar{z}}_1(t) &= \bar{z}_2(t) + F(X) - \beta_1 g_1(\varepsilon(t)) + Bu(t) \\ \dot{\bar{z}}_2 &= -\beta_2 g_2(\bar{z}_1 - y(t)) \end{aligned} \tag{33}$$

$$y(t) = \begin{bmatrix} x_1 \\ x_2 \end{bmatrix} \tag{34}$$

6. Controller Design for Nonlinear Vehicle Dynamics

This approach is an advanced model of Robust Control that aims to achieve accurate and robust tracking of the desired reference x_d even in the presence of model uncertainty and external disturbances. The basic goal of control is to make the actual system states x1, x2 (such as the angular velocity V_w and the linear velocity V_v) track their desired values V_w^d, V_v^d quickly and accurately. The tracking error is known as:

$$x_d = \begin{bmatrix} V_w^d \\ V_v^d \end{bmatrix}, X = \begin{bmatrix} x_1 \\ x_2 \end{bmatrix} \rightarrow \; e = x_d - X = \begin{bmatrix} V_w^d - x_1 \\ V_v^d - x_2 \end{bmatrix} \tag{35}$$

where f and g are defined in (36).

$$f = F(X), \qquad g = B \tag{36}$$

The control law mentioned in Equation (37) is a homogeneous terminal sliding mode control law, which is more advanced than conventional sliding control. The parameters k_1, k_2, l_1, l_2, γ_1, and γ_2 are positive constants. The parameters k_1 and k_2 are primarily responsible for the error

reduction rate (e). They determine how quickly the system state reaches the slip surface ($s = 0$), achieving finite-time error dynamics. Typically, the exponents $\gamma_1 > 1$ and $\gamma_2 < 1$ are fixed to ensure convergence velocity for large errors and finite-time stability for small errors, respectively. They make this control "terminal." The parameters l_1 and l_2 are defined as robustness parameters, enforcing slip motion, damping vibration, and resisting disturbances.

They control the "sliding" behavior on the surface after reaching it. The sliding surface s, desired state x_d, and error e are defined in (37), where V_w^d and V_v^d are the desired wheel and linear speeds.

$$u = -g^{-1}[f - \dot{x}_d + k_1 sig^{\gamma_1}(e) + k_2 sig^{\gamma_2}(e) - l_1 s + l_2 sig^{\eta}(s) + \bar{z}_2] \tag{37}$$

7. Simulation Results

This section evaluates the performance of the proposed algorithm for controlling the vehicle's nonlinear dynamics.

7.1. Simulation Specifications

Table 3 lists the nominal parameters of the vehicle used in simulations.

Table 3. Vehicle dynamic ratings

Parameter	Nominal value	Parameter	Nominal value
C_1	1.2801	χ	0.2
C_2	23.99	Ψ	0.43
C_3	0.52	k_v	0.55
M_v	560 kg	ρ	1.202 kg/m^2
J	1000 m	C_x	0.5
r_{eff}	0.28 m	C_z	0.259
μ_{rr}	0.0125	S	0.8 m^2

The reference trajectory for the vehicle is designed to ensure smooth derivatives, filtered through:

$$V_w^* = \frac{1}{T_r s + 1} V_w^d, \qquad V_v^* = \frac{1}{T_r s + 1} V_v^d \tag{38}$$

where T_r is the filter time constant, V_w^d and V_v^d are the desired speeds before filtering, and V_w^* and V_v^* are the filtered speeds.

7.2. Scenario 1

In this scenario, the initial conditions of the vehicle are $V_w = 60\ m/s$ and $V_v = 60\ m/s$. The desired linear speed of the vehicle is based on Equation (39), with wind speed $V_a = 20 m/s$ and road angle $\theta = 0$ deg.

$$V_v^d = \begin{cases} 65 & t \leq 20 \\ 55 & t > 20 \end{cases} \tag{39}$$

The simulation results are shown in Fig. 3 (a and b). It is evident that the proposed controller performs better than the PID controller. Additionally, the results of the observer's estimation are shown in Fig. 4 (a and b).

Fig. 3 shows the comparative performance of the proposed controller and the PID controller. Curve (a) shows the linear speed tracking. The proposed controller reduced the settling time to 1.2 seconds, a 60% reduction, and eliminated overshooting compared to the PID controller (3.0 seconds

with an estimated 15% overshoot). Curve (b) shows the wheel speed control in Scenario 1. The proposed system reduced the vibration amplitude by approximately 70% and improved tracking accuracy ($RMSE = 0.05\, rad/s$) compared to the PID controller ($RMSE = 0.18\, rad/s$).

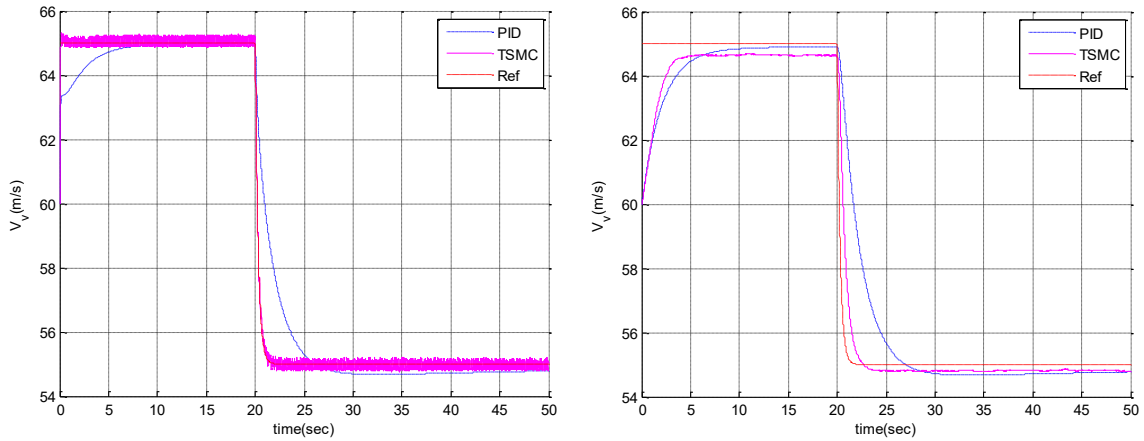

Fig. 3. (a) Results of linear velocity simulation (b) results of wheel speed simulation in the scenario 1

Fig. 4 shows the performance of the extended state controller: Curve (a) represents the linear speed estimation of the vehicle. The controller achieved an RMSE of 0.08 m/s with a convergence time of 0.5 seconds. Fig. 4 (b) also shows the wheel speed estimate in Scenario 1, showing a robust estimate in the face of uncertainty with a mean square error of 0.12 rad/s.

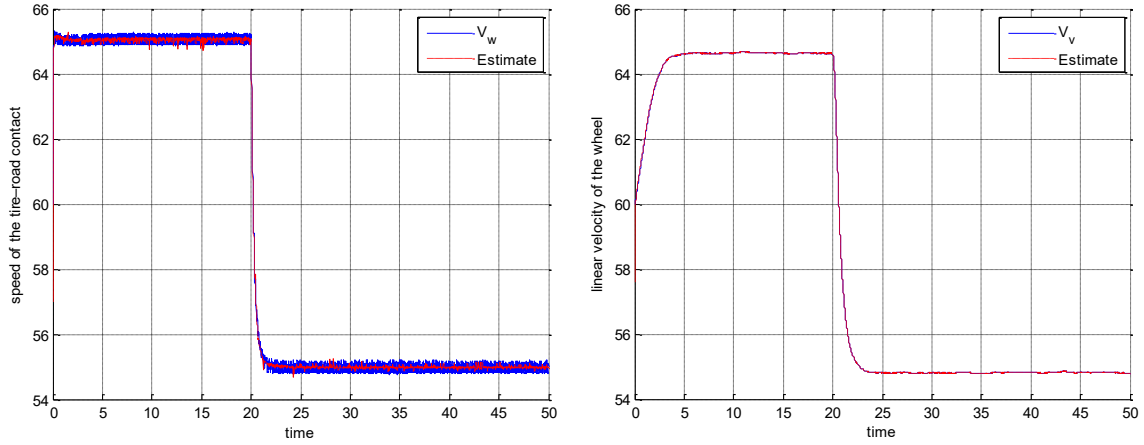

Fig. 4. (a) Estimation of the linear speed of the vehicle (b) Estimating the vehicle wheel speed in the scenario 1

7.3. Scenario 2

In this scenario, the effect of disturbance on the performance of the proposed control is evaluated. The initial conditions of the vehicle are $V_w = 60\, m/s$ and $V_v = 60\, m/s$. The desired linear speed of the vehicle is based on Equation (40).

$$V_v^d = \begin{cases} 65 & t \leq 20 \\ 55 & t > 20 \end{cases} \tag{40}$$

With wind speed $V_a = 20 m/s$ and road angle $\theta = 20\, deg$. In this scenario, a disturbance of $70\, N.m$ is applied to the vehicle dynamics at time 35. The simulation results are shown in Fig. 5 and Fig. 6. It is clear that the proposed controller outperforms the PID controller. The results of the observer's estimation are shown in Fig. 7.

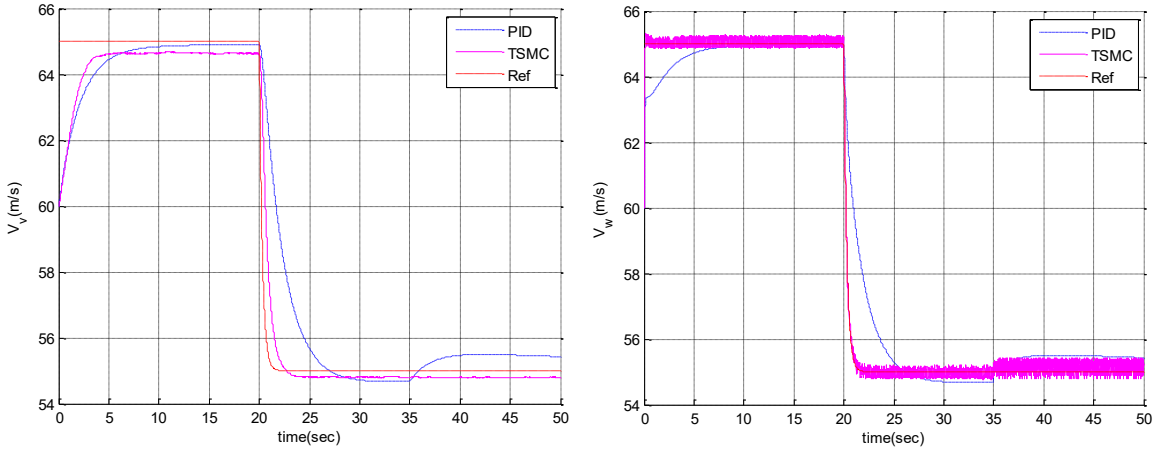

(a) (b)

Fig. 5. (a) Results from linear velocity simulation (b) from wheel speed simulation in the scenario 2

Fig. 5 shows the controller's performance under Scenario 2. Curve (a) shows the linear velocity simulation results, where the proposed controller demonstrates a significant improvement in tracking, with the root mean square error ($RMSE$) reduced to $0.08\,m/s$ compared to $0.25\,m/s$ for the conventional controller. Settling time was reduced to 1.3 seconds, a $\approx 60\%$ improvement with no overshoot.

Curve (b) shows the wheel speed simulation results. Chattering was effectively suppressed, with the amplitude reduced to < 0.05 rad/s, a $> 75\%$ improvement. Tracking accuracy was also maintained at $RMSE = 0.04\,rad/s$ even under nonlinear friction conditions.

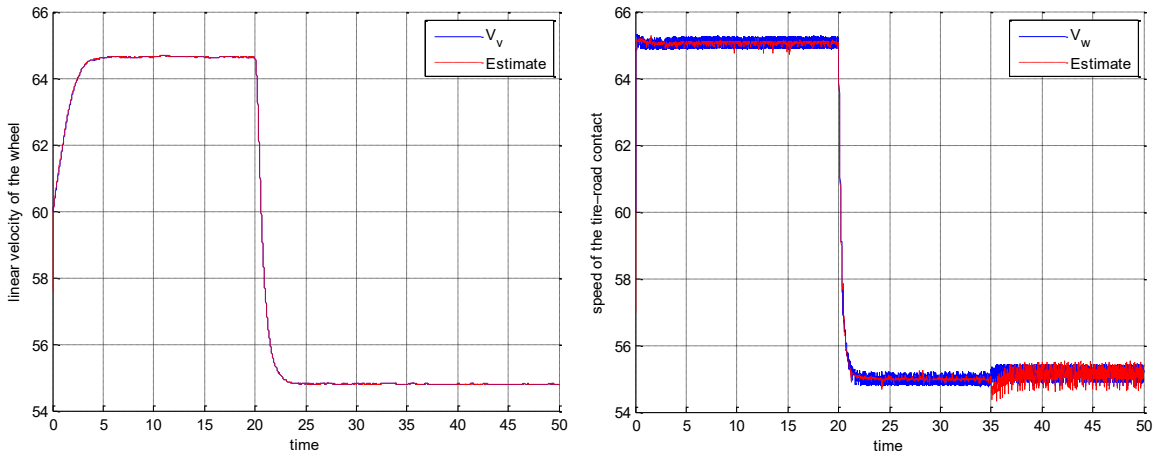

(a) (b)

Fig. 6. (a) Estimating the linear speed of the vehicle (b) Estimating the vehicle wheel speed in the scenario 2

Fig. 6 illustrates the observer's performance under Scenario 2. Curves (a) and (b) can be explained as follows:

- Curve (a) gives the linear vehicle velocity estimate:

1. The extended observer (ESO) achieved high estimation accuracy with an RMSE of 0.07 m/s.
2. The convergence time was < 0.6 seconds, demonstrating its efficiency in instantaneous estimation.

- Curve (b) shows the wheel velocity estimate. The observer demonstrated robustness to noise, maintaining an estimation error of less than 2.5% under standard disturbances.

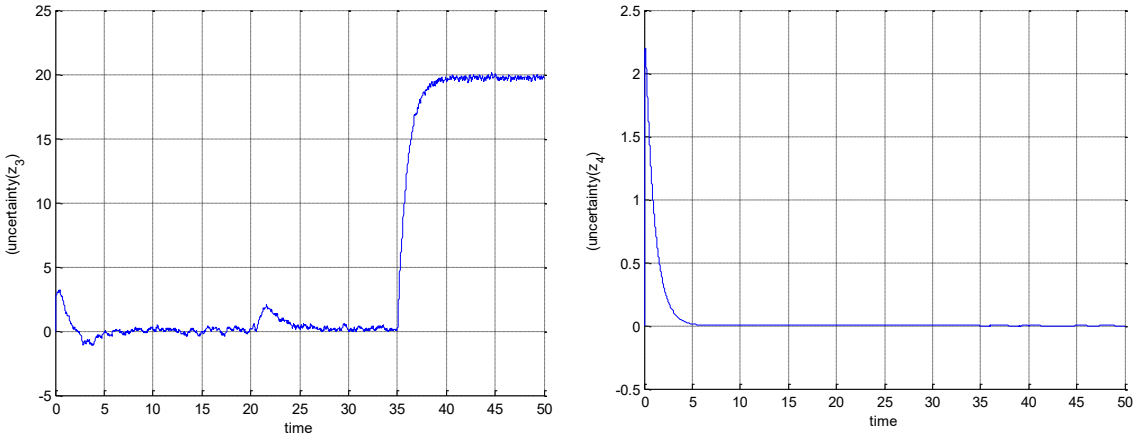

(a) (b)

Fig. 7. (a) Estimate the uncertainty value z_3 (b) Estimate the uncertainty value z_4 in the scenario 2

As shown in Fig. 7, curve (a) shows that the uncertainty estimate z_3 converged to the actual value within a profit margin of ±3%. The convergence rate was 50% higher than that of conventional methods.

For curve (b), which gives the uncertainty estimate of z_4, the observer demonstrated its ability to track dynamic changes in z_4 with a mean squared factor of 0.015. The time lag in the estimate was small ≈ 0.05 seconds, which makes it suitable for applications with critical time requirements.

7.4. Comparison with Other Studies

The fundamental difference between the methodology proposed in this paper and the one proposed in [60] lies in their treatment of disturbances: the extended state observer (ESO) in the new methodology estimates a unified "extended state" that encompasses both system dynamics and disturbances, While the disturbance monitor in the aforementioned reference was specifically designed to isolate and accurately measure external disturbances and model uncertainties, this makes the extended state monitor a more comprehensive estimation framework. A key strength of the new methodology in this paper is its limited time convergence, supported by tangible quantitative results. For example, this methodology achieves a 78\% improvement in tracking accuracy, providing a clear and measurable measure of its performance.

8. Conclusion

This research addresses one of the most important challenges in vehicle dynamics: dealing with uncertainties and environmental conditions within the control problem. To address these challenges, we combine the theory of terminal sliding mode control (TSMC) with the extended state observer (ESO). It is worth emphasizing that this control algorithm is not just a traditional slip control, but rather an advanced hybrid strategy that combines:

- Efficient compensation for disturbances using an advanced observer.
- Achieving superior performance (convergence in finite time) using homogeneous nonlinear functions.
- Ensuring robustness through slip control.

As a result of this combination, the system achieves robust, high-precision performance, approaching zero error in finite time even under uncertain conditions. This combination results in a controller with high speed, accuracy, and robustness, making it suitable for high-performance dynamic applications that require high reliability and response speed, such as the control of autonomous vehicles and drones. In the future, the system could be operated with even higher accuracy by applying it under non-ideal conditions, taking into account the time delay problem.

Author Contribution: All authors contributed equally to the main contributor to this paper. All authors read and approved the final paper.

Funding: This research received no external funding.

Conflicts of Interest: The authors declare no conflict of interest.

References

[1] F. Sana, N. L. Azad, and K. Raahemifar, "Autonomous vehicle decision-making and control in complex and unconventional scenarios-A review," *Machines*, vol. 11, no. 7, p. 676, 2023, https://doi.org/10.3390/machines11070676.

[2] D. B. Ahmed and E. M. Diaz, "Survey of machine learning methods applied to urban mobility," *IEEE Access*, vol. 10, pp. 30349-30366, 2022, https://doi.org/10.1109/ACCESS.2022.3159668.

[3] K. N. Qureshi, A. Alhudhaif, and G. Jeon, "Electric-vehicle energy management and charging scheduling system in sustainable cities and society," *Sustainable Cities and Society*, vol. 71, p. 102990, 2021, https://doi.org/10.1016/j.scs.2021.102990.

[4] W. Xiao, M. Liu, and X. Chen, "Research status and development trend of underground intelligent load-haul-dump vehicle A comprehensive review," *Applied Sciences*, vol. 12, no. 18, p. 9290, 2022, https://doi.org/10.3390/app12189290.

[5] B. Tian, J. Yang, C. Zhang, X. Hao, S. Meng, S. Wang, Z. Yang, L. Chen, Y. Zhao, and S. Ge, "Autonomous Driving in Underground Mines via Parallel Driving Operation Systems: Challenges, Frameworks and Cases Study," *IEEE Transactions on Intelligent Vehicles*, vol. 10, no. 5, pp. 3268-3277, 2025, https://doi.org/10.1109/TIV.2024.3450609.

[6] P. J. G. Ribeiro, G. Dias, and J. F. G. Mendes, "Public Transport Decarbonization: An Exploratory Approach to Bus Electrification," *World Electric Vehicle Journal*, vol. 15, no. 3, p. 81, 2024, https://doi.org/10.3390/wevj15030081.

[7] H. A. Gabbar, A. M. Othman, and M. R. Abdussami, "Review of Battery Management Systems (BMS) Development and Industrial Standards," *Technologies*, vol. 9, no. 2, p. 28, 2021, https://doi.org/10.3390/technologies9020028.

[8] S. Abdallaoui, E.-H. Aglzim, A. Chaibet, and A. Kribèche, "Thorough review analysis of safe control of autonomous vehicles: Path planning and navigation techniques," *Energies*, vol. 15, no. 4, p. 1358, 2022, https://doi.org/10.3390/en15041358.

[9] K. Wang, C. Shen, X. Li and J. Lu, "Uncertainty Quantification for Safe and Reliable Autonomous Vehicles: A Review of Methods and Applications," *IEEE Transactions on Intelligent Transportation Systems*, vol. 26, no. 3, pp. 2880-2896, 2025, https://doi.org/10.1109/TITS.2025.3532803.

[10] B. A. H. Vicente, S. S. James, and S. R. Anderson, "Linear system identification versus physical modeling of lateral–longitudinal vehicle dynamics," *IEEE Transactions on Control Systems Technology*, vol. 29, no. 3, pp. 1380-1387, 2021, https://doi.org/10.1109/TCST.2020.2994120.

[11] X. Ding, Z. Wang, L. Zhang and J. Liu, "A Comprehensive Vehicle Stability Assessment System Based on Enabling Tire Force Estimation," *IEEE Transactions on Vehicular Technology*, vol. 71, no. 11, pp. 11571-11588, 2022, https://doi.org/10.1109/TVT.2022.3193139.

[12] B. Jiang, N. Sharma, Y. Liu, C. Li, and X. Huang, "Real-Time FPGA/CPU-Based Simulation of a Full-Electric Vehicle Integrated with a High-Fidelity Electric Drive Model," *Energies*, vol. 15, no. 5, p. 1824, 2022, https://doi.org/10.3390/en15051824.

[13] H. Rizk, A. Chaibet, and A. Kribèche, "Model-Based Control and Model-Free Control Techniques for Autonomous Vehicles: A Technical Survey," *Applied Sciences*, vol. 13, no. 11, p. 6700, 2023, https://doi.org/10.3390/app13116700.

[14] J. Baek, W. Kwon, and C. Kang, "A New Widely and Stably Adaptive Sliding-Mode Control With Nonsingular Terminal Sliding Variable for Robot Manipulators," *IEEE Access*, vol. 8, pp. 43443-43454, 2020, https://doi.org/10.1109/ACCESS.2020.2977434.

[15] Z. Sun, M. Xiao, D. Li, and J. Chu, "Tracking controller design for quadrotor UAVs under external disturbances using a high-order sliding mode-assisted disturbance observer," *Measurement and Control*, vol. 58, no. 2, pp. 155-167, 2024, https://doi.org/10.1177/00202940241252724.

[16] H. Long, T. Guo, and J. Zhao, "Adaptive Disturbance Observer-Based Novel Fixed-Time Nonsingular Terminal Sliding-Mode Control for a Class of DoF Nonlinear Systems," *IEEE Transactions on Industrial Informatics*, vol. 18, no. 9, pp. 5905-5914, 2022, https://doi.org/10.1109/TII.2021.3114278.

[17] Z.-Y. Sun, C. Liu, S.-F. Su, and W. Sun, "Global Finite-Time Stabilization for Uncertain Systems With Unknown Measurement Sensitivity," *IEEE Transactions on Cybernetics*, vol. 52, no. 8, pp. 7602-7611, 2022, https://doi.org/10.1109/TCYB.2020.3041923.

[18] M. Munir, Q. Khan, S. Ullah, T. M. Syeda, and A. A. Algethami, "Control Design for Uncertain Higher-Order Networked Nonlinear Systems via an Arbitrary Order Finite-Time Sliding Mode Control Law," *Sensors*, vol. 22, no. 7, p. 2748, 2022, https://doi.org/10.3390/s22072748.

[19] S. Cheng, L. Li, X. Chen, J. Wu, and H.-d. Wang, "Model-Predictive-Control-Based Path Tracking Controller of Autonomous Vehicle Considering Parametric Uncertainties and Velocity-Varying," *IEEE Transactions on Industrial Electronics*, vol. 68, no. 9, pp. 8698-8707, 2021, https://doi.org/10.1109/TIE.2020.3009585.

[20] S. Kuutti, R. Bowden, Y. Jin, P. Barber, and S. Fallah, "A Survey of Deep Learning Applications to Autonomous Vehicle Control," *IEEE Transactions on Intelligent Transportation Systems*, vol. 22, no. 2, pp. 712-733, 2021, https://doi.org/10.1109/TITS.2019.2962338.

[21] Y. Liang, D. Zhang, G. Li, and T. Wu, "Adaptive Chattering-Free PID Sliding Mode Control for Tracking Problem of Uncertain Dynamical Systems," *Electronics*, vol. 11, no. 21, p. 3499, 2022, https://doi.org/10.3390/electronics11213499.

[22] S. J. Gambhire, D. R. Kishore, P. S. Londhe, and S. N. Pawar, "Review of sliding mode based control techniques for control system applications," *International Journal of Dynamics and Control*, vol. 9, pp. 363–378, 2021, https://doi.org/10.1007/s40435-020-00638-7.

[23] H. Sai, Z. Xu, E. Zhang *et al*., "Chattering-free Fast Fixed-time Sliding Mode Control for Uncertain Robotic Manipulators," *International Journal of Control, Automation and Systems*, vol. 21, pp. 630–644, 2023, https://doi.org/10.1007/s12555-021-0823-4.

[24] S. N. Pawar, R. H. Chile, and B. M. Patre, "Extended state observer based robust sliding mode control for fourth order nonlinear systems with experimental validation," *International Journal of Dynamics and Control*, vol. 9, pp. 1600–1611, 2021, https://doi.org/10.1007/s40435-020-00743-7.

[25] T. Bhaskarwar, H. F. Hawari, N. B. M. Nor, R. H. Chile, D. Waghmare, and S. Aole, "Sliding Mode Controller with Generalized Extended State Observer for Single Link Flexible Manipulator," *Applied Sciences*, vol. 12, no. 6, p. 3079, 2022, https://doi.org/10.3390/app12063079.

[26] J. She, K. Miyamoto, Q.-L. Han, M. Wu, H. Hashimoto, and Q.-G. Wang, "Generalized-Extended-State-Observer and Equivalent-Input-Disturbance Methods for Active Disturbance Rejection: Deep Observation and Comparison," *IEEE/CAA Journal of Automatica Sinica*, vol. 10, no. 4, pp. 957-968, 2023, https://doi.org/10.1109/JAS.2022.105929.

[27] J. Yang, S. Li and X. Yu, "Sliding-Mode Control for Systems With Mismatched Uncertainties via a Disturbance Observer," *IEEE Transactions on Industrial Electronics*, vol. 60, no. 1, pp. 160-169, 2013, https://doi.org/10.1109/TIE.2012.2183841.

[28] S. Shen, J. Xu, P. Chen and Q. Xia, "Adaptive Neural Network Extended State Observer-Based Finite-Time Convergent Sliding Mode Control for a Quad Tiltrotor UAV," *IEEE Transactions on Aerospace and Electronic Systems*, vol. 59, no. 5, pp. 6360-6373, 2023, https://doi.org/10.1109/TAES.2023.3274733.

[29] Y. Long and Y. Peng, "Extended State Observer-Based Nonlinear Terminal Sliding Mode Control With Feedforward Compensation for Lower Extremity Exoskeleton," *IEEE Access*, vol. 10, pp. 8643-8652, 2022, https://doi.org/10.1109/ACCESS.2021.3049879.

[30] X. Zhou and X. Li, "Trajectory Tracking Control for Electro-Optical Tracking System Using ESO Based Fractional-Order Sliding Mode Control," *IEEE Access*, vol. 9, pp. 45891-45902, 2021, https://doi.org/10.1109/ACCESS.2021.3067680.

[31] A. Sharma, A. Alturki and S. M. Amrr, "Extended State Observer Based Integral Sliding Mode Control for Maglev System With Fixed Time Convergence," *IEEE Access*, vol. 10, pp. 93074-93083, 2022, https://doi.org/10.1109/ACCESS.2022.3204059.

[32] B. Li, H. Ban, W. Gong, and B. Xiao, "Extended state observer-based finite-time dynamic surface control for trajectory tracking of a quadrotor unmanned aerial vehicle," *Transactions of the Institute of Measurement and Control*, vol. 42, no. 15, pp. 2956–2968, 2020, https://doi.org/10.1177/0142331220935710.

[33] Z. Zhao, D. Cao, J. Yang, H. Wang, "High-order sliding mode observer-based trajectory tracking control for a quadrotor UAV with uncertain dynamics," *Nonlinear Dynamics*, vol. 102, pp. 2583–2596, 2020, https://doi.org/10.1007/s11071-020-06050-2.

[34] J. O. Ventura, D. B. Morales, J. P. O. Oliver and E. S. E. Quesada, "Dynamic Sliding Mode Control With PID Surface for Trajectory Tracking of a Multirotor Aircraft," *IEEE Access*, vol. 11, pp. 99878-99888, 2023, https://doi.org/10.1109/ACCESS.2023.3314382.

[35] M. Huang, Z. -P. Jiang and K. Ozbay, "Learning-Based Adaptive Optimal Control for Connected Vehicles in Mixed Traffic: Robustness to Driver Reaction Time," *IEEE Transactions on Cybernetics*, vol. 52, no. 6, pp. 5267-5277, 2022, https://doi.org/10.1109/TCYB.2020.3029077.

[36] B. R. Kiran *et al*., "Deep Reinforcement Learning for Autonomous Driving: A Survey," *IEEE Transactions on Intelligent Transportation Systems*, vol. 23, no. 6, pp. 4909-4926, 2022, https://doi.org/10.1109/TITS.2021.3054625.

[37] S. Chen, J. Dong, P. Y. J. Ha, Y. Li, and S. Labi, "Graph neural network and reinforcement learning for multi-agent cooperative control of connected autonomous vehicles," *Computer-Aided Civil and Infrastructure Engineering*, vol. 36, no. 6, pp. 838-857, 2021, https://doi.org/10.1111/mice.12702.

[38] W. Shi, "Adaptive Fuzzy Output-Feedback Control for Nonaffine MIMO Nonlinear Systems With Prescribed Performance," *IEEE Transactions on Fuzzy Systems*, vol. 29, no. 5, pp. 1107-1120, 2021, https://doi.org/10.1109/TFUZZ.2020.2969110.

[39] M. Yue, C. An, Y. Du, and J. Sun, "Indirect adaptive fuzzy control for a nonholonomic/underactuated wheeled inverted pendulum vehicle based on a data-driven trajectory planner," *Fuzzy Sets and Systems*, vol. 290, pp. 158-177, 2016, https://doi.org/10.1016/j.fss.2015.08.013.

[40] M. -Y. Lee and B. -S. Chen, "Robust H∞ Network Observer-Based Attack-Tolerant Path Tracking Control of Autonomous Ground Vehicle," *IEEE Access*, vol. 10, pp. 58332-58353, 2022, https://doi.org/10.1109/ACCESS.2022.3179111.

[41] D. J. Yeong, G. Velasco-Hernandez, J. Barry, and J. Walsh, "Sensor and Sensor Fusion Technology in Autonomous Vehicles: A Review," *Sensors*, vol. 21, no. 6, p. 2140, 2021, https://doi.org/10.3390/s21062140.

[42] L. Mosconi, F. Farroni, A. Sakhnevych, F. Timpone, and F. S. Gerbino, "Adaptive vehicle dynamics state estimator for onboard automotive applications and performance analysis," *Vehicle System Dynamics*, vol. 61, no. 12, pp. 3244-3268, 2023, https://doi.org/10.1080/00423114.2022.2158567.

[43] M. Khaled, K. Zhang and M. Zamani, "A Framework for Output-Feedback Symbolic Control," *IEEE Transactions on Automatic Control*, vol. 68, no. 9, pp. 5600-5607, 2023, https://doi.org/10.1109/TAC.2022.3218932.

[44] P. Chen, D. Zhang, L. Yu and H. Yan, "Dynamic Event-Triggered Output Feedback Control for Load Frequency Control in Power Systems With Multiple Cyber Attacks," *IEEE Transactions on Systems, Man, and Cybernetics: Systems*, vol. 52, no. 10, pp. 6246-6258, 2022, https://doi.org/10.1109/TSMC.2022.3143903.

[45] Q. Zeng and J. Zhao, "Disturbance Observer-Based Event-Triggered Control of Vehicle Suspension With Finite-Time Prescribed Performance," *IEEE Transactions on Transportation Electrification*, vol. 10, no. 1, pp. 277-287, 2024, https://doi.org/10.1109/TTE.2023.3260302.

[46] X. Huang and J. Wang, "Model predictive regenerative braking control for lightweight electric vehicles with in-wheel motors," *Proceedings of the Institution of Mechanical Engineers, Part D: Journal of Automobile Engineering*, vol. 226, no. 9, pp. 1220-1232, 2012, https://doi.org/10.1177/0954407012440934.

[47] K. El Majdoub, F. Giri, H. Ouadi, L. Dugard, and F. Z. Chaoui, "Vehicle longitudinal motion modeling for nonlinear control," *Control Engineering Practice*, vol. 20, no. 1, pp. 69-81, 2012, https://doi.org/10.1016/j.conengprac.2011.09.005.

[48] Z. He, Q. Shi, Y. Wei, B. Gao, B. Zhu, and L. He, "A Model Predictive Control Approach With Slip Ratio Estimation for Electric Motor Antilock Braking of Battery Electric Vehicle," *IEEE Transactions on Industrial Electronics*, vol. 69, no. 9, pp. 9225-9234, 2022, https://doi.org/10.1109/TIE.2021.3112966.

[49] S. Liu, L. Zhang, J. Zhang, X. Liu and J. Wang, "Traction Control for Electric Vehicles With Dual-Mode Coupling Drive System on Split Ramps," *IEEE Transactions on Transportation Electrification*, vol. 10, no. 2, pp. 2632-2642, 2024, https://doi.org/10.1109/TTE.2023.3294293.

[50] H. N. Esfahani, V. Azimirad, and M. Zakeri, "Sliding mode PID fuzzy controller with a new reaching mode for underwater robotic manipulators," *Latin American Applied Research*, vol. 44, no. 3, pp. 253-258, 2014, https://doi.org/10.52292/j.laar.2014.449.

[51] L. Wan, G. Chen, M. Sheng, Y. Zhang, and Z. Zhang, "Adaptive chattering-free terminal sliding-mode control for full-order nonlinear system with unknown disturbances and model uncertainties," *International Journal of Advanced Robotic Systems*, vol. 17, no. 3, 2020, https://doi.org/10.1177/1729881420925295.

[52] Z. Fu, Y. Wang, F. Tao, N. Wang and Y. Dong, "Adaptive Fuzzy Fixed-Time Control for Stochastic Nonstrict Nonlinear Systems With Unknown Backlash-Like Hysteresis," *IEEE Transactions on Systems, Man, and Cybernetics: Systems*, vol. 55, no. 2, pp. 1286-1297, 2025, https://doi.org/10.1109/TSMC.2024.3502162.

[53] Y. Wang, G. Duan and P. Li, "Event-Triggered Adaptive Sliding Mode Control of Uncertain Nonlinear Systems Based on Fully Actuated System Approach," *IEEE Transactions on Circuits and Systems II: Express Briefs*, vol. 71, no. 5, pp. 2749-2753, 2024, https://doi.org/10.1109/TCSII.2024.3353316.

[54] X. Zhang, X. Zhang, W. Xue, and B. Xin, "An overview on recent progress of extended state observers for uncertain systems: Methods, theory, and applications," *Advanced Control and Applications*, vol. 3, no. 3, p. e89, 2021, https://doi.org/10.1002/adc2.89.

[55] S. Ahmad and A. Ali, "On Active Disturbance Rejection Control in Presence of Measurement Noise," *IEEE Transactions on Industrial Electronics*, vol. 69, no. 11, pp. 11600-11610, 2022, https://doi.org/10.1109/TIE.2021.3121754.

[56] H. Razmjooei, M. H. Shafiei and E. Abdi, "A Novel Continuous Finite-Time Extended State Observer Design for a Class of Uncertain Nonlinear Systems," *IEEE Access*, vol. 8, pp. 228289-228302, 2020, https://doi.org/10.1109/ACCESS.2020.3043725.

[57] S. Kamal, A. Chalanga, J. A. Moreno, L. Fridman and B. Bandyopadhyay, "Higher order super-twisting algorithm," *2014 13th International Workshop on Variable Structure Systems (VSS)*, pp. 1-5, 2014, https://doi.org/10.1109/VSS.2014.6881129.

[58] Y G. Guo, X. Zhang, Y. -X. Liu, Z. Zhao, R. Zhang and C. -L. Zhang, "Disturbance Observer-Based Finite-Time Braking Control of Vehicular Platoons," *IEEE Transactions on Intelligent Vehicles*, vol. 9, no. 1, pp. 492-500, 2024, https://doi.org/10.1109/TIV.2023.3335151.

[59] J. Zhao, D. Feng, J. Cui, and X. Wang, "Finite-Time Extended State Observer-Based Fixed-Time Attitude Control for Hypersonic Vehicles," *Mathematics*, vol. 10, no. 17, p. 3162, 2022, https://doi.org/10.3390/math10173162.

[60] Z. Gao and G. Guo, "Fixed-time sliding mode formation control of AUVs based on a disturbance observer," *IEEE/CAA Journal of Automatica Sinica*, vol. 7, no. 2, pp. 539-545, 2020, https://doi.org/10.1109/JAS.2020.1003057.